Emission cross sections for electron impact on Cl_2

R. Scott Schappe and Kyle Wendt
Department of Physics, Lake Forest College, Lake Forest, Illinois 60045, USA
(Received 22 May 2007; published 15 August 2007)

We have measured the absolute emission cross section for the Cl_2^+ $A\ ^2\Pi_u$–$X\ ^2\Pi_g$ system for 10–750 eV electrons incident on chlorine molecules. The cross section for the system possesses a broad peak at 100 eV of 2.0×10^{-16} cm^2, typical of such ionization processes. At this energy, the A-X cross section is responsible for two-thirds of the total Cl_2^+ production and one-third of the total ionization cross section. We also measured the emission cross section from 7 to 740 eV for the 307 nm system of Cl_2. The energy dependence of the cross section indicates that the excitation is to a Cl_2 $^1\Sigma_u^+$ or $^1\Pi_u$ state with a decay to a repulsive potential.

DOI: 10.1103/PhysRevA.76.022707 PACS number(s): 34.80.Gs

I. INTRODUCTION

The primary technological motivation to study chlorine is the plasma processing of semiconductors, in which Cl_2^+ ions are of particular importance [1,2]. Despite this significance, there has been remarkably little work on electron-Cl_2 collision cross sections. Mass spectrometry has been used to measure absolute total ionization cross sections [3] and the relative production rates for the various chlorine ions [4]. But no emission cross sections for electron impact on Cl_2 are found in the literature. The spectroscopic work on chlorine is also incomplete. Huberman observed a high-frequency discharge at high resolution to identify 42 vibrational transitions of the $^{35}Cl_2^+$ $A\ ^2\Pi_u$–$X\ ^2\Pi_g$ system [5]. Tuckett and Peyerimhoff extended this work using a supersonically cooled chlorine beam excited by electrons to isolate 117 different vibrational transitions of $^{35}Cl_2^+$ [6]. The spectroscopic investigation found that the Cl_2^+ $A\ ^2\Pi_u$ state is strongly perturbed, which has prevented the assignment of vibrational quantum numbers to levels in that state. Furthermore, the identifications of some of the emission systems of chlorine are inconclusive. The paucity of experimental work is at least in part due to the difficulty in working with such a reactive gas. Spectral analysis is also complicated by the isotopic ratio of chlorine: approximately 25% is ^{37}Cl, while the remainder is ^{35}Cl, and the resulting isotope shifts effectively triple the number of transitions present in the natural Cl_2 spectrum.

II. EXPERIMENT

A. Apparatus

The experimental apparatus and procedure have been previously described in more detail [7]. Briefly, research-grade chlorine gas is slowly admitted into a collision chamber (with a throughput of about 1×10^{-3} Pa m^3/s), from which it is simultaneously pumped away at the same rate. This minimizes the buildup of contaminants produced by the reaction of the chlorine with the collision chamber and electron gun surfaces. The pressure of the gas is measured by a capacitance manometer and is typically between 0.1 and 0.7 mtorr within the collision chamber. The electron gun uses a tungsten wire as the electron emitter in place of the indirectly heated BaO cathode described in Ref. [7], which cannot function in the chlorine environment. The electron beam is collected by a Faraday cup and the fluorescence caused by the electron collisions emerges though a slot in the side of the cup. The emitted light is dispersed by a 1/4 m monochromator and detected by a photomultiplier tube (C31034A-02) in a photon-counting mode. A computer controls the monochromator and electron energy, and it retrieves information from the manometers, electrometer (for the electron current), and photon counter.

B. Method

We determine the absolute emission cross sections using the optical method [7,8]. Briefly, monoenergetic electrons collide with the chlorine molecules and excite and ionize them. We detect the emitted radiation as these excited molecules decay. The absolute optical emission cross section Q_{em} is proportional to the fluorescence intensity emitted by the excited molecules. Additionally, the cross section depends on the target density (n), the electron flux (j), the solid angle subtended by the collection optics (Ω), and the optical efficiency (ε) of the detection system. The last we determine by replacing the electron beam signal with a lamp of known spectral irradiance. For the simplest case of unpolarized emission from a uniform density target,

$$Q_{\mathrm{em}} = \frac{4\pi e}{\Omega \Delta x \Delta\lambda n I} S, \tag{1}$$

where I is the total electron beam current, Δx is the viewed length of the electron beam, $\Delta\lambda$ is the monochromator bandpass, and e is the magnitude of the electron charge. The absolute emission signal S (counts nm/s), is the experimental intensity I_{em} divided by the efficiency and then integrated over the transition:

$$S = \int \frac{I_{\mathrm{em}}}{\varepsilon} d\lambda. \tag{2}$$

Graphically, S is the area under the band on the emission signal versus wavelength plot, when the efficiency of the detection system has been folded in.

The chlorine reacts with the metal surfaces within the collision chamber and the resulting by-products (e.g., FeCl) would build up to unacceptable levels if we used a static gas target. Instead, we slowly flow the gas through the chamber

as described in Sec. II A. At this flow rate the target density within the volume where the collisions occur is essentially constant (as opposed to a molecular beam). However, the actual target number density n will be slightly different from the density determined by a nearby capacitance manometer, though proportional to it. To determine the chlorine target number density we use a relative flow technique [7,9]. In addition to the chlorine data, we separately measure emission from the N_2^+ first negative (0,0) band at 391 nm using identical pressures in the gas reservoir upstream of the collision chamber. The nitrogen cross section is the average of the 100 eV peak cross sections compiled by Doering and Yang [10], which is 17.1×10^{-18} cm^2 at 100 eV.

Using Eq. (1) for each gas, the relation between the unknown chlorine cross section Q_{Cl} and the known cross section for the nitrogen calibration gas Q_{N} is

$$Q_{\mathrm{Cl}} = Q_N \frac{S_{\mathrm{Cl}}}{S_{\mathrm{N}}} \frac{n_{\mathrm{N}}}{n_{\mathrm{Cl}}}, \tag{3}$$

where S is the relative integrated emission signal from Eq. (2) for the nitrogen calibration gas or chlorine, and n_{N} and n_{Cl} represent the number densities of the respective target gases within the collision region.

At the low pressures in the collision chamber (about 0.5 mtorr), the dc drift of the manometer during the experiment can significantly affect the pressure measurements, so we also measure the pressure in the reservoir, where the pressures are much higher (60–120 mtorr) and easier to measure reliably. Repeated careful experimental measurements show that for 100 mtorr of chlorine in the reservoir, the pressure at the chamber manometer is 0.58 ± 0.02 mtorr; for 100 mtorr of nitrogen in the reservoir, the chamber manometer reads 0.47 ± 0.02 mtorr. Under our experimental conditions, the chamber pressure is also linearly dependent on the pressure in the reservoir. Additionally, the signal is linearly proportional to the pressure measured within the collision chamber and to the electron beam current.

To corroborate the result of our pressure measurements, we also calculated the steady-state collision chamber pressure using a gas-flow model [11]. In this experiment, the flow rate from the reservoir through a tube into the collision chamber is equal to the flow rate out of the chamber through the small area of the nearly closed gate valve above the diffusion pump. The flow into the chamber is in the transition regime and so is a combination of molecular and viscous flow. The viscous flow is proportional to the molecular diameter squared and this is the cause of the difference in chamber pressures between the two gases given the same reservoir pressures. For our calculations we use diameters from the empirical relationship for homonuclear diatomic molecules [12], $d_0=R_e+0.23$, where R_e is the equilibrium bond length (in nm). The flow out of the chamber is in the molecular flow regime. Equating the two flow rates for a 100 mtorr reservoir pressure and a 0.001 mtorr diffusion pump pressure yields a chamber pressure of 0.53 mtorr for Cl_2 and 0.46 mtorr for N_2. These are in good agreement with our experimental numbers, particularly given the lack of good molecular diameter data for chlorine, and serve to confirm that our experimental results are reasonable. Recasting Eq. (3) in favor of the more robust reservoir pressure, we apply our experimentally determined correction factor of 1.23 (0.58 mtorr/0.47 mtorr):

$$Q_{\mathrm{Cl}} = Q_{\mathrm{N}} \frac{S_{\mathrm{Cl}}}{S_{\mathrm{N}}} \left(\frac{p_{\mathrm{res,N}}}{1.23 p_{\mathrm{res,Cl}}} \right). \tag{4}$$

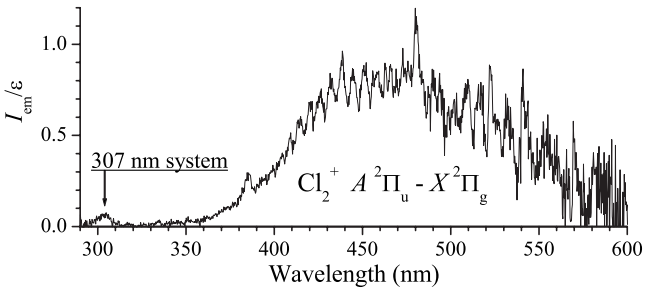

FIG. 1. Emission spectrum for 90 eV electrons on Cl_2. The 300-nm-blazed grating necessary to observe the 307 nm system suffers a loss of efficiency at longer wavelengths and causes the noise shown in the data. Other data were also taken with a 600-nm-blazed grating to improve the signal at longer wavelengths.

C. Spectrum

A typical emission spectrum is shown in Fig. 1. The dominant feature is the Cl_2^+ $A\ ^2\Pi_u$–$X\ ^2\Pi_g$ system, which is also responsible for the characteristic blue color of the chlorine discharge. Even at relatively high resolution, the large number of rotational transitions present at room temperature broadens each vibrational transition so that it significantly overlaps its neighboring bands, forming a broad peak from 350 to 600 nm. Thus, apportioning the total area of the broad peak among the 117 identified $^{35}Cl_2^+$ vibrational transitions and their equivalents for the other isotopic mixtures is very difficult.

Nevertheless, knowing the individual vibrational transition cross sections would be valuable, so we attempted other less direct means to extract these measurements. Fitting such a large number of overlapping bands, using theoretically guided emission band shapes, is viable only when the spectroscopic data are quite good and the bands are somewhat distinct [7]. We hoped that it would be possible instead to fit families of transitions emitted from a common vibrational level of the $A\ ^2\Pi_u$ state, which could be constructed from the spectroscopic data and the branching fractions. Unfortunately, no experimental branching fractions are available, so we attempted to calculate them using the potential curves from Ref. [13]. However, the perturbation of the A state is too severe, and the eigenvalues of the A-state vibrational levels were not in good agreement with the experimental spectroscopic data. The perturbation is manifest primarily as an irregularity in the upper-state vibrational energy level series. The exact source of this perturbation is not completely understood. In their spectroscopic investigations, Huberman [5] and Tuckett and Peyerimhoff [6] propose several possibilities, the most likely of which is an interaction with the $^2\Sigma_u^+$ and $^2\Delta_u$ states, which are similar in energy and internu-

TABLE I. Absolute emission cross sections for electron impact on Cl_2. The Cl_2^+ cross section has a total uncertainty of 20%; the 307 nm system has an uncertainty of 25%.

System	Onset (eV)	Energy of maximum cross section (eV)	Maximum cross section (cm^2)
$A\ ^2\Pi_u - X\ ^2\Pi_g$	14.1±0.2	100	2.0×10^{-16}
307 nm	9.6±0.4	80	1.0×10^{-18}

clear equilibrium distance. The similarity in r_e suggests the possibility of a vibrational interaction, which could explain the irregular vibrational series, but an interaction with non-Π states would cause a stronger Q branch than they observed. The work of Tuckett and Peyerimhoff points to a homogeneous spin-orbit interaction ($\Omega=0$) with these Σ and/or Δ states, which may explain why $A\ ^2\Pi_{u,1/2}$ and $A\ ^2\Pi_{u,3/2}$ are perturbed differently.

The inability to obtain branching fractions for the vibrational transitions of the A-X system prevents us from untangling the Gordian knot of the overlapping vibrational transitions in our spectrum, so we present only a total cross section for the system. Since the A state can decay only to the X state, this is also the total cross section for the $A\ ^2\Pi_u$ state.

In addition to the A-X system we also observed the emission system at 307 nm, which was discovered in 1947 by Venkateswarlu [14]. There are also many atomic lines listed in the 300–600 nm region, though we could not observe them in our spectra, so we assume that their contribution to the total cross section is negligible.

D. Results

1. A-X system

Table I presents the cross sections for the two observed systems. The Cl_2^+ $A\ ^2\Pi_u - X\ ^2\Pi_g$ system is by far the largest, with a maximum total cross section of 2.0×10^{-16} cm^2 occurring at about 100 eV. The onset of 14.1±0.2 eV (at 435 nm) agrees with the potential for the $A\ ^2\Pi_u$ state calculated by Peyerimhoff and Buenker [13] shown in Fig. 2, as well as with previous experimental data [15–17].

Figure 3 shows the energy dependence of the emission cross section for this system, which has the broad peak that is typical of ionization excitation, though there is also the suggestion of another smaller peak at 40 eV. Within our experimental uncertainty, we could detect no polarization of the A-X emission. Our total estimated uncertainty for this cross section is 20%, which is a quadrature combination of a 15% uncertainty in the N_2 calibration cross section, a 10% uncertainty in S, and 8% for the number density correction.

As mentioned earlier, molecular ions play a vital role in plasma processing. Figure 4 shows the recommended total ionization cross section [3] along with our A-X system cross section for incident electron energies up to 200 eV. The energy dependence of the A-X system is very similar to that of the total ionization cross section, which is not surprising since the A-X system is a significant contributor to the total ion production, producing about one-third of all ions for electron energies above 25 eV. The energy dependencies of our data and the total ionization cross section also display subpeaks at about 35–40 eV, the source of which is unknown, though it may be related to the perturbation of the $A\ ^2\Pi_u$ state.

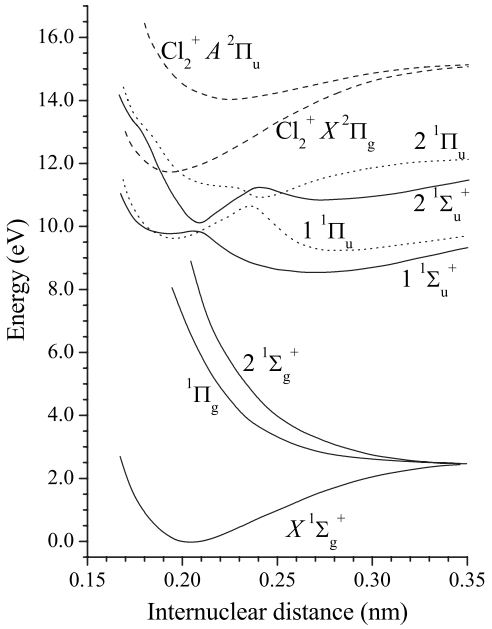

FIG. 2. Potential energy diagram for some of the electronic states relevant to this work (from Ref. [13]).

In Fig. 4 we have also included the total cross section for the production of Cl_2^+ ions alone. We determined this by combining the recommended total ionization data of Ref. [3] with the data for the relative production of all ionic chlorine species that contribute to the total ionization cross section: Cl_2^+, Cl^+, and Cl^{2+} [4]. The total ionization cross section is normally defined as the sum of the individual ion cross sections weighted by their ionic charge:

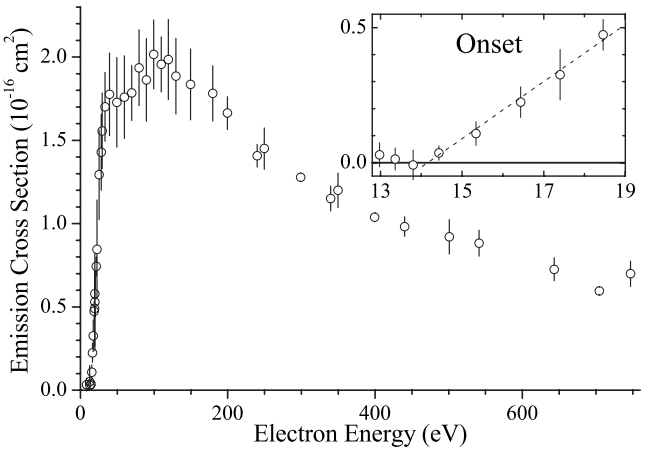

FIG. 3. Excitation function for the $A\ ^2\Pi_u - X\ ^2\Pi_g$ system at 435 nm. The error bars indicate only the statistical uncertainty. The inset shows the onset behavior.

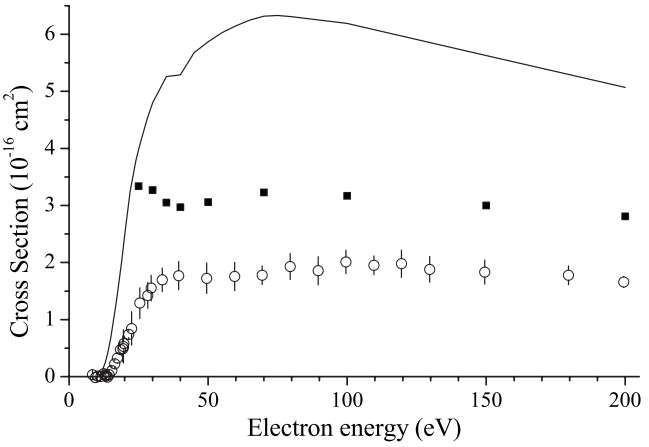

FIG. 4. Total ionization cross section from Ref. [3] (–), total Cl_2^+ cross section calculated from the data in Refs. [3,4] (■), and the A-X system cross section (○).

$$\sigma_{\text{tot}} = \sigma_{Cl_2^+} + \sigma_{Cl^+} + 2\sigma_{Cl^{2+}}.$$

This can be rewritten using the relative production rates for Cl^+ and Cl^{2+} relative to Cl_2^+ measured as a function of energy in Ref. [4]:

$$\sigma_{\text{tot}} = \sigma_{Cl_2^+} + \alpha\sigma_{Cl_2^+} + 2\beta\sigma_{Cl_2^+},$$

which can be rearranged to express the Cl_2^+ cross section in terms of the known experimental quantities. As shown in Fig. 4, the A-X system accounts for almost two-thirds of the Cl_2^+ formed by electron collision at energies greater than 40 eV. At higher energies the A-X system and the Cl_2^+ cross section have similar energy dependencies, but at threshold the Cl_2^+ cross section has a sharp peak, indicating the presence of at least one other ion production channel. This is most likely the direct ionization into the $X\ ^2\Pi_g$ ground state.

2. 307 nm system

Our work on the 307 nm system helps to shed light on its origins. In Ref. [14], Venkateswarlu originally identified this transition as an excitation to a $^3\Sigma_u^+$ state with a subsequent decay to $^1\Sigma_g^+$. Our observations do not support this initial designation. Figure 5 shows the energy dependence of the cross section for the 307 nm system. The Cl_2^+ ground state has a measured electron excitation threshold of 11.6 eV [17]. Thus the measured excitation function onset of 9.6±0.4 eV for the system is too low for an ionization process. This, combined with the broad peak and $\ln(E)/E$ energy dependence of the cross section at higher energies, indicates that the upper Cl_2 state is optically connected to the $X\ ^1\Sigma_g^+$ ground

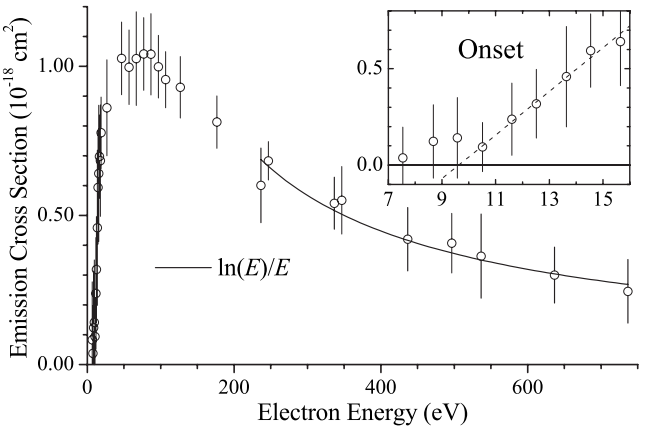

FIG. 5. Excitation function for the 307 nm system. The error bars indicate only the statistical uncertainty. At high energies, the cross section displays the $\ln(E)/E$ dependence characteristic of optically allowed excitation. The inset shows the onset behavior.

state: a $^1\Sigma_u^+$ or $^1\Pi_u$. Figure 2 shows some of these candidate potentials taken from Peyerimhoff and Buenker [13]. Those authors note that the $^1\Sigma_u^+$ manifold is more strongly optically connected to the ground state than the $^1\Pi_u$ states, though the energy of the lowest $^1\Pi_u$ state is in better agreement with our onset measurements. From the energy of the emitted photons, the lower state is clearly one or more of the repulsive potentials shown lying 2–3.5 eV below the upper state. Peyerimhoff and Buenker also state that the electronic transition moment is expected to change rapidly with internuclear distance, so the Franck-Condon principle of vertical transitions does not apply. Thus the vibrational wave functions of either well of the 1 $^1\Pi_u$ state would be accessible from the ground state.

III. CONCLUSION

The excitation from the neutral ground state into the $A\ ^2\Pi_u$–$X\ ^2\Pi_g$ system is the dominant pathway for the production of Cl_2^+ ions for electron collision energies above 40 eV and it is responsible for more than one-third of all chlorine ions above 25 eV. Unfortunately, the dense and heavily overlapping spectrum precludes the measurement of individual vibrational transitions, which might help to shed light on the important, but highly perturbed, $A\ ^2\Pi_u$ state. It would be valuable to measure the relative vibrational transition cross sections using a supersonically cooled chlorine target. This would isolate these transitions, thus providing the branching fractions necessary to better understand the $A\ ^2\Pi_u$ state and to allow the apportionment of the total system cross section among the vibrational transitions.

[1] V. M. Donnelly, D. L. Flamm, and G. Collins, J. Vac. Sci. Technol. **21**, 817 (1982).
[2] J. A. Levinson, E. S. Shaqfeh, M. Balooch, and A. V. Hamza, J. Vac. Sci. Technol. B **18**, 172 (2000).
[3] L. G. Christophorou and J. K. Olthoff, J. Phys. Chem. Ref. Data **28**, 131 (1999).
[4] P. Calandra, C. S. S. O'Connor, and S. D. Price, J. Chem. Phys. **112**, 10821 (2000).

[5] F. P. Huberman, J. Mol. Spectrosc. **20**, 29 (1966).
[6] R. P. Tuckett and S. D. Peyerimhoff, Chem. Phys. **83**, 203 (1984).
[7] R. S. Schappe and E. Urban, Phys. Rev. A **73**, 052702 (2006).
[8] A. R. Filippelli, C. C. Lin, L. W. Anderson, and J. W. McConkey, Adv. At., Mol., Opt. Phys. **33**, 1 (1994).
[9] M. A. Khakoo, T. Jayaweera, S. Wang, and S. Trajmar, J. Phys. B **26**, 4845 (1993).
[10] J. P. Doering and J. Yang, J. Geophys. Res. **101**, 19723 (1996).
[11] John F. O'Hanlon, *A User's Guide to Vacuum Technology*, 2nd ed. (Wiley, New York, 1989), Chap. 3.
[12] S. H. Kang and J. A. Kunc, J. Phys. Chem. **95**, 6971 (1991).
[13] S. D. Peyerimhoff and R. J. Buenker, Chem. Phys. **57**, 279 (1981).
[14] P. Venkateswarlu, Proc. Indian Acad. Sci., Sect. A **26**, 22 (1947).
[15] A. W. Potts and W. C. Price, Trans. Faraday Soc. **67**, 1242 (1971).
[16] A. B. Cornford, D. C. Frost, C. A. McDowell, J. L. Ragle, and I. A. Stenhouse, J. Chem. Phys. **54**, 2651 (1971).
[17] D. C. Frost and C. A. McDowell, Can. J. Chem. **38**, 407 (1960).